Error estimation and accurate mapping based ALE formulation for 3D simulation of friction stir welding

Simon Guerdoux, Lionel Fourment

Error Estimation And Accurate Mapping Based ALE Formulation For 3D Simulation Of Friction Stir Welding

Simon Guerdoux, Lionel Fourment*

CEMEF, Mines de Paris, BP 207, 06 904 Sophia Antipolis Cedex, France
** corresponding author: lionel.fourment@ensmp.fr*

Abstract. An Arbitrary Lagrangian Eulerian (ALE) formulation is developed to simulate the different stages of the Friction Stir Welding (FSW) process with the FORGE3® F.E. software. A splitting method is utilized: a) the material velocity/pressure and temperature fields are calculated, b) the mesh velocity is derived from the domain boundary evolution and an adaptive refinement criterion provided by error estimation, c) P1 and P0 variables are remapped. Different velocity computation and remap techniques have been investigated, providing significant improvement with respect to more standard approaches. The proposed ALE formulation is applied to FSW simulation. Steady state welding, but also transient phases are simulated, showing good robustness and accuracy of the developed formulation. Friction parameters are identified for an Eulerian steady state simulation by comparison with experimental results. Void formation can be simulated. Simulations of the transient plunge and welding phases help to better understand the deposition process that occurs at the trailing edge of the probe. Flexibility and robustness of the model finally allows investigating the influence of new tooling designs on the deposition process.

Keywords: ALE, Simulation, Friction Stir Welding, Error Estimation.

INTRODUCTION

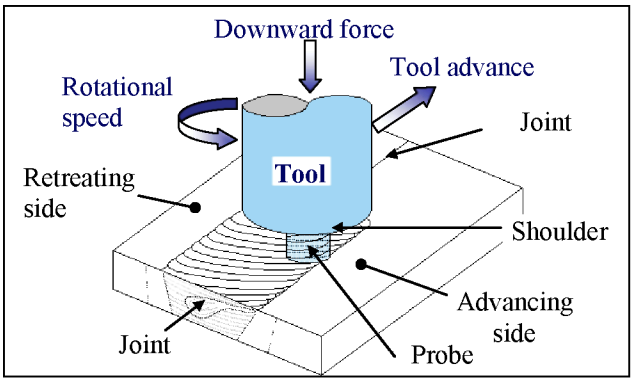

FIGURE 1. Welding phase of FSW process.

In the Friction Stir Welding (FSW) process, the plunging phase is followed by a stationary heating step which prepares the actual welding phase, which is shown in Figure **1**. The simulation of plunging and of possible defects (voids) formation during welding require accurately computing free surface movements while very large deformations take place under the tool. This issue is tackled by appealing to an Arbitrary Lagrangian Eulerian (ALE) formulation, which is used both for quasi Lagrangian plunging and quasi Eulerian welding. It is implemented into the FORGE3® FE software [1], using a splitting method [2]. Treatment of convective terms and calculation of the mesh velocity have always been the two main difficulties of this approach. Efforts have been done to improve the adaptive mesh velocity calculation and the utilized remap techniques to deal with convective terms. The improved formulation allows entire FSW process simulation. This work reports on numerical results that the improved software provides in FSW simulation.

LAGRANGIAN STEP

FORGE3® is extensively used to simulate hot, warm and cold forging of 3D geometry parts, using a pure Lagrangian formulation [1]. At each time step, it solves the thermal and mechanical equations, which constitute the first step of the implemented ALE splitting method [2].

The weak form of the momentum and incompressibility equations result into a mixed velocity-pressure formulation that is discretized by an enhanced (P1+/P1) quasi-linear interpolation based on 4-noded tetrahedron elements. Viscoplastic, elasto-

CP908, *NUMIFORM '07, Materials Processing and Design: Modeling, Simulation and Applications*
edited by J. M. A. César de Sá and A. D. Santos

plastic and elasto-viscoplastic constitutive equations can be utilized to model material deformations with elastic spring back and residual stresses. Contact is handled by a penalty formulation, and friction conditions at the interface between part and tools are modeled by Tresca, Coulomb or Norton friction laws. Furthermore, additional models are introduced to more precisely describe the evolution of rheological and tribological parameters with temperature.

The discretized form of the heat equation is solved at each time step using an incremental coupling with the mechanical equations. This equation is also solved in FSW tool and backing plate in order to better simulate thermal boundary effect. Heat generated by material deformation and by friction with the tool, thermal exchanges by conduction, convection and radiation, are thus taken into account to simulate all welding phenomena.

ALE SPLITTING FORMULATION

The second step of the ALE splitting method consists in computing the mesh velocity $\boldsymbol{w}$, which can be different from the material one. $\boldsymbol{w}$ is computed to optimize the elements quality and increase the computation accuracy, independently from the material deformation.

The final step of the method consists in dealing with the convective terms, which appear in time grid derivatives of any variable φ through the following relationship.

$$\frac{d_g \varphi}{dt} = \dot{\varphi} + (\boldsymbol{w} - \boldsymbol{v}).\nabla\varphi \qquad (1)$$

Adaptive Mesh Velocity Calculation

Global formulation

The mesh velocity $\boldsymbol{w_n}$ of any node is calculated by an iterative centering algorithm. Equation (2) provides the location of any node n. Its grid velocity is deducted from equation (3), at any iteration it.

$$\boldsymbol{x}_n^{it} = \frac{1}{|\Gamma_n|}\sum_{e\in\Gamma_n} \boldsymbol{x}_{ge}^{\,it-1} C_e^{it-1} \qquad (2)$$

$$\boldsymbol{w}_n^{it} = \frac{(\boldsymbol{x}_n^0 - \boldsymbol{x}_n^{it})}{\Delta t} \qquad (3)$$

where Γ_n is the set of elements contiguous to node n (i.e. which contain n), $\boldsymbol{x}_{ge}$ is the barycenter of element e. C_e^{it-1} is a weight factor that is defined in [3]. It combines geometrical and adaptive considerations to provide fully regularized mesh with controlled elements qualities and optimize element size.

Surface conditions

The calculation of the grid velocity through the iterative algorithm is conditioned by the conservation equation on the boundaries. $\boldsymbol{w}$ must satisfy:

$$(\boldsymbol{w} - \boldsymbol{v}).\boldsymbol{n} = \boldsymbol{0} \qquad (4)$$

where $\boldsymbol{v}$ is the material velocity and $\boldsymbol{n}$ is either a consistent normal to the workpiece on the free surface [2] or the outside contact normal. For points belonging to edges or similar zones, a local modal analysis allows selecting additional vectors to properly enforce the consistency condition in noticeable directions. Equation (4) is enforced at any boundary node for each selected normal directions by:

$$\boldsymbol{w}_n = \boldsymbol{w}_n^{it} - \left((\boldsymbol{v} - \boldsymbol{w}_n^{it}).\boldsymbol{n}\right).\boldsymbol{n} \qquad (5)$$

In order to minimize volume diffusion due to the difference between tangential grid velocity and tangential material velocity, a projection procedure has been added. The updated node $\boldsymbol{x}_{\mathrm{M}}^{\mathrm{it}}$ is orthogonally projected onto its patch P_m, the set of elements connected to node M:

$$\boldsymbol{x}_{\mathrm{M_p}}^{\mathrm{it}} = \Pi_{\mathrm{P_m}}(\boldsymbol{x}_{\mathrm{M}}^{\mathrm{it}}) \qquad (6)$$

A new material velocity $\boldsymbol{v}_{\mathrm{M_p}}^{\mathrm{it}}$ and a new penalizing normal $\tilde{\boldsymbol{n}}_{\mathrm{M_p}}^{\mathrm{it}}$ are then interpolated from the nodes of the facet f containing the projected point M_P:

$$\begin{cases} \tilde{\boldsymbol{n}}_{M_P}^{it} = \displaystyle\sum_{n\in f} N_n\left(\boldsymbol{v}_{M_P}^{it}\right)\tilde{\boldsymbol{n}}_{\boldsymbol{n}} \Big/ \left\| \sum_{n\in f} N_n\left(\boldsymbol{v}_{M_P}^{it}\right)\tilde{\boldsymbol{n}}_{\boldsymbol{n}} \right\| \\ \boldsymbol{v}_{M_P}^{it} = \displaystyle\sum_{n\in f} N_n\left(x_{M_P}^{it}\right) v_n \end{cases} \qquad (7)$$

The resulting mesh velocity for node m is then computed as:

$$\boldsymbol{w}_{\boldsymbol{m}}^{it} = \frac{\boldsymbol{x}_{\boldsymbol{m}} - \boldsymbol{x}_{M_p}}{\Delta t} + \boldsymbol{w}_{M_p} \qquad (8)$$

with $\boldsymbol{w}_{\mathrm{M_p}} = \boldsymbol{v}_{\mathrm{M_p}}^{\mathrm{it}}.\tilde{\boldsymbol{n}}_{\mathrm{M_p}}^{\mathrm{it}}$

This projection procedure clearly reduces free-surface oscillations.

Variable Remapping Step

A Lagrangian like transport has been preferred to tackle the convective terms. In order to ensure accurate remapping of piecewise discontinuous (P0) variables (stress field tensor σ and equivalent strain $\bar{\varepsilon}$), like nodal linear continuous (P1) variables, a new remap technique has been implemented. It is based on Liska-Orkisz Finite Differences Method and Superconvergent Patch Recovery technique (SPR) [6]. It consists in computing the gradient of the variable on element centered patches (for P0 variables) or on nodal

centered patches (for P1 variables), as illustrated in 2D in Figure **2**. Considering the stress remap, for example, a recovered continuous solution $\tilde{\boldsymbol{\sigma}}_h^k$ is directly constructed on element centered patches from Lagrangian values at integration points. The local second order polynomial expansion of $\tilde{\boldsymbol{\sigma}}_h^k$ is written on each patch:

$$\tilde{\boldsymbol{\sigma}}_h^k(x,y,z) = \boldsymbol{P}.\boldsymbol{a}^k \qquad (9)$$

with $\begin{cases} \boldsymbol{P} = (1, x, y, z, x^2, y^2, z^2, xy, xz, yz) \\ \boldsymbol{a}^k = (a_1^k, a_2^k, a_3^k, a_4^k, a_5^k, a_6^k, a_7^k, a_8^k, a_9^k, a_{10}^k)^t \end{cases}$

The consistency of the remapping operator requires that $\tilde{\boldsymbol{\sigma}}_h^k$ is equal to $\boldsymbol{\sigma}_h^k$ at the centre of the patch, so that $\boldsymbol{a}_1^k$ is equal to $\boldsymbol{\sigma}_h^k$. The other coefficients are determined by minimizing the following least square expression on the patch:

$$\Pi(\boldsymbol{a}^k) = \sum_{i=1}^{NG} \left(\boldsymbol{\sigma}_h(i) - \tilde{\boldsymbol{\sigma}}_h^k(x_i, y_i, z_i)\right)^2 \qquad (10)$$

where NG is the number of integration points (of nodes, in case of nodal variables) of the patch. If this number is insufficient to provide a well conditioned system, the patch is enlarged with second order neighbors (for P0 variables), or the expansion order is reduced (for P1 variables). The remapped values at ALE integration points are obtained by inverse interpolation of (9), with the patch centered at the nearest Lagrangian integration point.

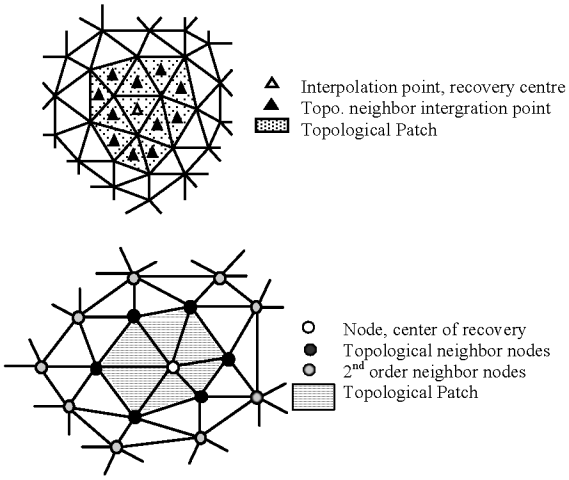

FIGURE 2. 2D illustration of element centered patches (top) and nodal centered patches (bottom).

Benchmark Tests and First Applications

Several benchmark tests have been developed to check the robustness of the adaptive mesh velocity computation, evaluate the efficiency of the implemented transport techniques and obtain quantitative comparisons with more classical techniques. They show that the implemented method is significantly more efficient [3].

The improved ALE formulation has also been utilized for significantly different material forming processes. Figure **3** shows successful simulations of adiabatic shearing in high speed orthogonal metal cutting, and of reaching stationary state in 3D plate rolling. These results show the robustness, versatility and efficiency of the proposed formulation.

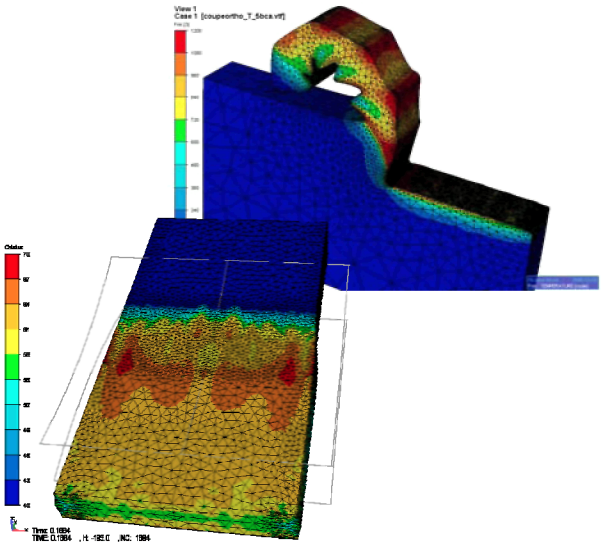

FIGURE 3. Temperature field: in high speed orthogonal metal cutting with adiabatic shearing (top right) and in 3D cold plate rolling (a steady state is reached).

NUMERICAL RESULTS OF FSW SIMULATION

The main objective of this work is to develop a robust formulation to accurately simulate the entire Friction Stir Welding process. Therefore, the ultimate validations of proposed techniques consist in the simulation of the different steps of the process and in comparisons with experimental results.

Steady Welding State: Friction Coefficient Identification

Firstly, processing experiments have been conducted at the Brigham Young University by Sean Darby to provide experimental welding data in order to compare with numerical simulations of the stationary welding phase. A first calibration is carried out for the friction coefficients through welding forces.

Experimental set-up

The experimental workpiece consisted of a 279mm by 457mm panel in AA6061, which was 9.53 mm thick. A 15.9 mm (0.625 in) thick liquid-cooled aluminum cooling plate was used to remove thermal energy from the workpiece. A 4.76 mm (0.1875 in) thick steel anvil was placed on its top for protection and to give a solid backing surface for the workpiece.

The tool used for this study was manufactured from heat-treated H13 tool steel. Its dimensions consisted of a shoulder diameter of 25.4 mm (1.0 in), body length (from the top of the tool to the shoulder) of 83.8 mm (3.3 in), shoulder concavity angle of 8 degrees. It was 6.35 mm (0.25 in) length and 4.8 mm not including the portion that extended into the concave shoulder cavity. Three thermocouples were located in the FSW tool: one at the tip of the pin, one at the root of the pin and one at the tip of the shoulder. The tool is unthreaded and was tilted of 2.5 degrees.

The plate was friction stir processed (bead on plate) on a retrofitted Kearney & Trecker knee mill with PLC/PC control and data acquisition system. Forces, motor power, shoulder depth, and temperatures in the tool are recorded at 50 millisecond intervals. After the preliminary experimental plunge phase, the prescribed plunge depth was about 0.25mm with control feedback of the effective plunge depth. The tool was then allowed to dwell for about 1 s. The spindle speed for dwelling and welding remained at 650 rpm. During the 120 s welding experiment, the plunge depth is manually adjusted in order to maintain a quasi-constant axial force on the tool.

Model specifications

Contrary to the tool, the modelled workpiece has not exactly the experimental dimensions. It is 150 mm large, 300 mm long, and 9.53 mm thick. It is assumed that the distance from the tool to the edges of the plate is long enough to not modify the thermal field in the vicinity of the tool.

The constitutive behaviour of the workpiece material was elasto-viscoplastic. The material consistency and the strain rate sensitivity, providing the yield stress, were tabulated in function of the temperature in order to fit hot and cold Hansel-Spitel laws provided by the Forge3® material data base.

A thermal computation is performed inside the FSW tool and the backing plate. The thermal characteristics of the AA6061 workpiece, the H13 tool, and the backing plate are assumed constant. They are summarized in table 1 along with the utilized exchange coefficients. A preliminary plunging phase simulation had provided the initial temperature map (see Figure 4).

In order to model the clamping system, two symmetry plans are applied on lateral sides of the workpiece. The transverse velocity 3,39mm/s is prescribed as an inflow velocity (see Figure 4).The FSW tool and the anvil have a rigid body movement.

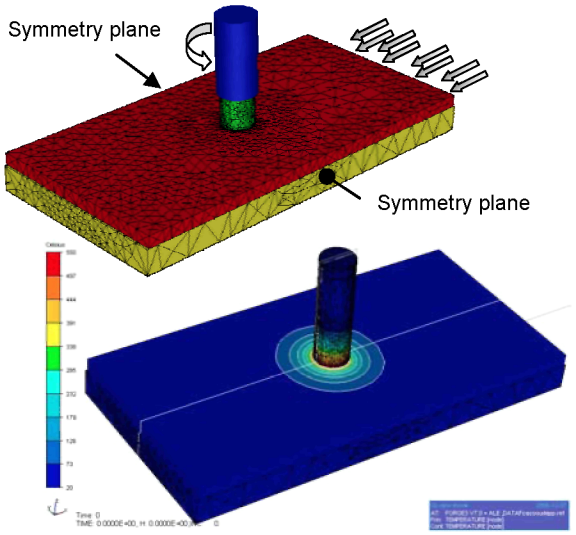

FIGURE 4. Global view of the model and initial temperature field (resulting from a preliminary plunging simulation).

The contact between the tool and the workpiece is a simulation result. In fact, the friction law determines the intensity of the shear stress at the contact interface between tool and workpiece, so the workpiece nodes get in or out of contact according to the material flow. The friction law is crucial to the global FSW model. The utilized viscoplastic friction law connects the frictional shear stress $\boldsymbol{\tau}_f$ to the sliding velocity $\Delta \boldsymbol{v}_s$ as follows:

$$\boldsymbol{\tau}_f = -\alpha_f K_{(T)} \left\| \Delta \boldsymbol{v}_s \right\|^{q-1} \Delta \boldsymbol{v}_s \qquad (11)$$

In order to identify the two coefficients α_f and q, three simulations have been carried out with different values:

- case 1: $\alpha_f = 0.4$ and $q = 0.1$
- case 2: $\alpha_f = 0.3$ and $q = 0.125$
- case 3: $\alpha_f = 0.4$ and $q = 0.125$

Making few simplification hypotheses, by neglecting the movements of the free surfaces that is estimated from previous ALE calculations, the Eulerian formulation provides a robust and fast way to simulate the steady welding state (as illustrated in Figure 5) and identify friction parameters.

TABLE 1. Thermal characteristics of the modelled materials.

	Conductivity λ (W/m.°K)	Thermal capacity c (J/kg.°K)	Density ρ (kg/m^3)	Emissivity	Exchange coefficient h_c (W/m^{-2}.°K^{-1})
Workpiece AA6061	180	896	2700	0.05	50000 / FSW tool, 2000 / anvil, 30 / air at 20°C
FSW Tool H13	24.3	460	7850	0.88	20000 / tool holder at 15°C, 20 / air at 20°C
Anvil	250	1230	2800	0.05	2000 / cooling plate 15°C, 30 / air at 20°C

First Results

The tool forces (*Fz* in the axial direction and *Fx* in the traverse direction), which have been experimentally measured and averaged among four welds), are compared with the simulated ones for each considered case, and the results are presented in Table 2. It is noticeable how sensitive to friction coefficients the results are.

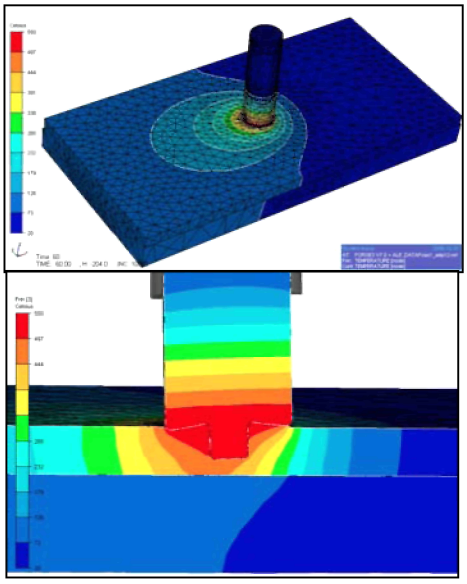

FIGURE 5. Global temperature map (on top) and temperature field in the cross joint section (on bottom) obtained at steady state (after 60 s of welding) in case 3.

TABLE 2. Experimentally measured tool forces and simulated ones in the three frictional cases at steady welding state.

	Vertical force Fz (kN)	Traverse force Fx (kN)
Experience	24	4
Simulated case 1	40,5	10
Simulated case 2	34.5	7.5
Simulated case 3	24	5

The couple of friction parameters (α_f = 0.4 ; q = 0.125) provides the best results. The axial torque and the tool temperatures also compare well to the experimental results, but the differences between the three simulated cases are less significant.

Then, simulation of the steady welding state allows observing the material stream lines, as in figure **6** for case 3.

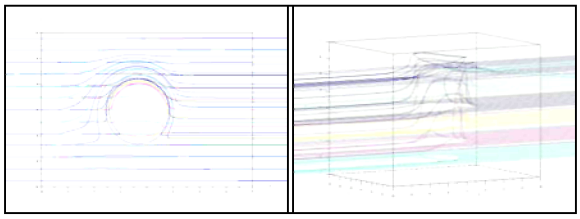

FIGURE 6. Visualization of transverse and axial movements of Lagrangian particles in the vicinity of the FSW tool at steady state (Stream Lines).

Transient Welding Phases

Often ignored in literature, the simulation of the transient states of the FSW process is made possible with the proposed ALE formulation.

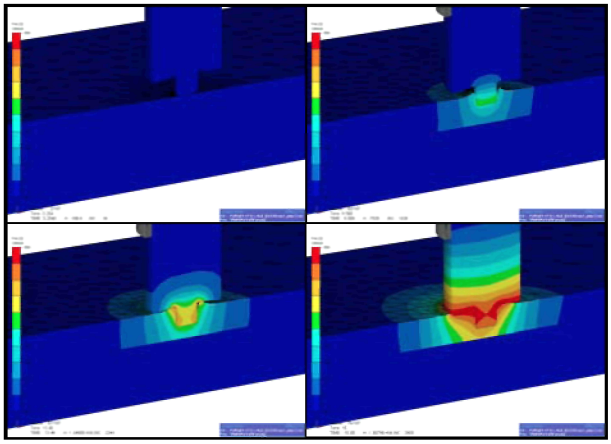

FIGURE 7. Temperature field during the plunging phase (cross section view).

Plunging Phase

The simulation of the plunging phase provides a good initial loading state, which is necessary to simulate the dwelling and welding phases. The obtained temperature map compares well with experimental values.

Transient Welding and Void Formation

The utilized numerical model allows studying all transient phenomena such as flash formations or deposition process (see Figure 8). It has made it possible to show that a void can be generated at the bottom trailing edge of the pin when the initial temperature of the material or the initial loading state of the tool is too low. Robust management of the mesh during void collapsing and huge flash formation remains however one issue to persue.

FIGURE 8. Simulation with flash formation (on left) and void generation (cross section view on right) during welding.

Tooling Design

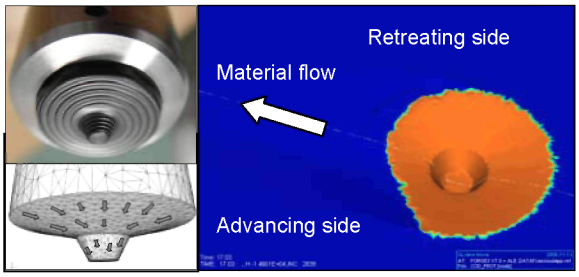

FIGURE 9. Welding simulation with new tooling design (threads on convex shoulder and conical probe)

The flexibility of the model provides many possibilities to study new tooling designs. The influence of tool threads on material flow and heating is modeled by an additional virtual frictional velocity, which is applied perpendicularly to threads during the contact analysis. Figure 9 shows the foot print of a new tool after 17 s of welding simulation. In this case, a void is generated if the influence of threads is not taken into account.

CONCLUSION

A new adaptive ALE formulation has been developed in the Forge3 software. It allows accurately simulating of all steps of the Friction Stir Welding process: plunge, dwell and weld. In order to become fully predictive, a couple of friction coefficients for a viscoplastic law has been directly identified from steady welding experimental forces. Therefore, transient welding phases or phenomena, such as plunge phase, or deposition process and void formation, can be simulated for a more accurate evaluation of the process conditions. The flexibility of the model also allows comparing different tool designs for process optimization.

ACKNOWLEDGEMENT

The authors acknowledge financial support for this work from the Office of Naval Research, contract N° N00014-03-1-0792, Dr. Julie Christodoulou, Program Manager.

REFERENCES

1. J.– L. Chenot, L. Fourment, Finite Element Simulation of the Forging Process: Future developments, in: M. Pietrzyk, Z. Mitura, K. J. Eds.5th ESAFORM conference Akademia Gorniczo-Hutnicza, 2002.
2 M. Bellet, V. Fachinotti D., ALE method for solidification modelling, Computer-methods-in-applied-mechanics-and-engineering 193 n (39-41), (2004) 4355-4381.
3 L. Fourment, S. Guerdoux., Enhanced transport and remeshing schemes for ALE formulations: application to numerical simulation of Friction Stir Welding, ESAFORM 2006, Akapit publisher, Krakow, Poland, 75-78 (2006)
4 A. Huerta, F. Casadei, J. Donea, An arbitrary Lagrangian-Eulerian stress update procedure for coining, in: J. L. Chenot , O. C. Zienkiewicz Eds.Numerical Methods in Industrial Forming Processes 1992.
5. H. Schmidt and J. Hattel, "A local model for the thermomechanical conditions in friction stir welding", *Modelling Simul. Mater. Sci. Eng.*, **13**, 77-93 (2004).
6. O. C. Zienkiewicz, J. Z. Zhu, "The superconvergent patch recovery (SPR) and adaptive finite element refinement", *Comput. Methods Appl. Mech. Eng.* **101** (1992) 207-224.